

Investigation of Site Characterization and Vulnerability in Antakya (Turkey) under Basin Effect

Aydın Büyüksaraç¹, Özcan Bektaş^{2*}, Ercan Işık³, Semir Över⁴, Selçuk Kaçın⁴

¹ Çan Vocational School, Çanakkale Onsekiz Mart University, Çanakkale, Türkiye

^{2*} Department of Geophysical Engineering, Sivas Cumhuriyet University, Sivas, Türkiye

³ Department of Civil Engineering, Bitlis Eren University, Bitlis, Türkiye

⁴ Department of Civil Engineering, İskenderun Technical University, İskenderun-Hatay, Türkiye

Received: 14/03/2022, **Revised:** 02/09/2022, **Accepted:** 12/10/2022, **Published:** 31/08/2023

Abstract

It is very important and necessary to know the depth of the bedrock in determining the soil behavior. However, determining the depth of bedrock spatially is a very difficult and costly process. The depth of the bedrock can be obtained by using the dominant vibration frequency obtained by the microtremor data. The bedrock depth map was created with the correlation produced from the dominant vibration frequencies obtained from microtremor measurements made in Antakya (Turkey). In bedrock calculations at low frequencies, the value range shows scattering. In the vulnerability analysis for Antakya soils, a low level of vulnerability Index ($K_g = 6$) was obtained in the east and northeast of the area. It has been observed that the S-wave velocity (V_s) in this area is lower than 406 ms^{-1} . In this case, this value has been accepted as the vulnerability threshold value in Antakya soils. Peak Ground Acceleration (PGA) and Peak Ground Velocity (PGV) were obtained for each location by using earthquake ground motion levels with 2%, 10%, 50%, and 68% probability of exceedance in 50-year periods. The PGA values in the region range from 0.43 to 0.47 g for earthquakes with a return period of 475 years.

Keywords: Bedrock, Microtremor, Vulnerability Index, Predominant period, Antakya

Havza Etkisi Altında Antakya'da (Türkiye) Alan Karakterizasyonu ve Hasar Görebilirliğin İncelenmesi

Öz

Zemin davranışının belirlenmesinde anakaya derinliğinin bilinmesi çok önemli ve gereklidir. Ancak anakayanın derinliğini belirlemek çok zor ve maliyetli bir süreçtir. Anakayanın derinliği, mikrotremor verilerinden elde edilen baskın titreşim frekansı kullanılarak saptanabilir. Anakaya derinlik haritası, Antakya'da (Türkiye) yapılan mikrotremor ölçümlerinden elde edilen baskın titreşim frekanslarından üretilen korelasyon ile oluşturulmuştur. Düşük frekanslarda anakaya hesaplamalarında değer aralığı saçılma göstermektedir. Antakya zemini için yapılan hasar görebilirlik analizinde alanın doğu ve kuzeydoğusunda düşük seviyede ($K_g = 6$) hassasiyet elde edilmiştir. Bu alandaki S dalgası hızının (V_s) 406 ms^{-1} 'den daha düşük olduğu gözlemlenmiştir. Böylece, bu değer Antakya zemini için hassasiyet eşik değeri olarak kabul edilmiştir. Her bir lokasyon için 50 yıllık periyotlarda %2, %10, %50 ve %68 aşılma olasılıklı deprem yer hareketi seviyeleri kullanılarak En Büyük Yer İvmesi (PGA) ve En Büyük Yer Hızı (PGV) elde edilmiştir. Tekrarlanma periyodu 475 yıl olan depremler için bölgedeki PGA değerleri 0,43 ile 0,47 g arasında değişmektedir.

Anahtar Kelimeler: Anakaya, Mikrotremor, Hasar görebilirlik, Baskın periyod, Antakya

*Corresponding Author: obektas@cumhuriyet.edu.tr

Aydın BÜYÜKSARAÇ, <https://orcid.org/0000-0002-4279-4158>

Özcan BEKTAŞ, <https://orcid.org/0000-0001-5232-4654>

Ercan IŞIK, <https://orcid.org/0000-0001-8057-065X>

Semir ÖVER, <https://orcid.org/0000-0002-5604-4956>

Selçuk KAÇIN, <https://orcid.org/0000-0001-5406-5756>

1. Introduction

Determining the seismic risk of any region is an integral part of modern pre-earthquake disaster management. Factors such as local ground conditions, earthquake history, fault and fault groups in the region, characteristics of faults and earthquake characteristics directly affect seismic hazard analysis. Briefly, local soil conditions and seismicity elements of the region will directly change the spectrum and its characteristics [1-7].

When the soft soil layer is defined on the hard bedrock, the horizontal movement reveals amplification properties in the ground. Thus, the high value of the horizontal-to-vertical spectral ratio (HVSr) will be possible if the horizontal spectrum (H) gets a strong frequency value and the frequency of the vertical spectrum (V) remains lower. Considering the dynamic conditions, while there are body waves that usually damage and have high energy during an earthquake, the slow motion of the body waves in this area is likely to transfer more energy to surface waves due to repeated reflections. Thus, especially Rayleigh waves are transformed from non-destructive to destructive. Rayleigh waves will propagate most effectively in which frequency range is defined as the dominant frequency (f_0) [8]. This technique, have been extensively studied by many researchers to measure the site effects such as amplification, ambient noise produced by soft ground layers in certain frequency bands [9-26]. Soil behavior analysis depends not only on the geomorphology and properties of the subterranean soil layers, but also on the bedrock type and location. The bedrock location greatly influences the seismic response and the bedrock type influences the one-dimensional ground response analysis. As the depth of the sole increases, the amplification at high frequency decreases, for the lower frequency the amplification increases. Peak ground acceleration (PGA) increases with increasing bedrock velocity, ie bedrock with higher shear wave velocity.

In order to fully define the behavior in a site, the surface and deep morphology of that site must be well known. The seismic response at the surface of soil deposits is dependent mainly on the frequency content and amplitude of ground motion at the bedrock. In particular, the distance of soils from bedrock is one of the most important factors determining earthquake ground behavior [27]. This situation, as explained above, should be determined by the harmony between the bedrock and soft soil layers. The seismic response on the surface of soft soils mainly depends on the frequency content and amplitude of the ground motion in the bedrock [27- 29]. Thus, it is important to define the engineering bedrock, soil, soil transfer function, dynamic loads on the site and the possible stress-strain relationships that may occur due to these loads in order to define the soil behaviors that occur under dynamic loads [30]. Many researchers have conducted experimental approaches to calculate deep structure, especially bedrock depth, using nonlinear regression relationships from surface data [27]. However, derived relationships often yield field specific results. Most of these studies aimed to obtain bedrock depth from the dominant frequency values.

In this study, the depth values obtained from Refraction microtremor (ReMi) measurements were used to calculate the coefficients of the formula developed to calculate the bedrock depth. Since depth changes of up to 100 meters can be easily observed here, it has been appropriate to use it as an application technique for soils with less bedrock depth such as Antakya. Thus, it

provides convenience for the practitioners and the opportunity to check the accuracy of the results. On the other hand, the soil behavior of Antakya was also examined in terms of Vs30 velocity distribution obtained from ReMi measurements. At the same time, Peak Ground Acceleration (PGA) and Peak Ground Velocity (PGV) were calculated using earthquake ground motion levels for each ReMi location for earthquakes with a 2%, 10%, 50% and 68% probability of exceedance over a 50-year period.

2. Geological Information of Antakya

Antakya is located in the western end of the Turkey-Syria border about 1000 km in length. The Asi River divides the city into two parts and poured out the Mediterranean. Antakya settlement is found on both sides of the Asi River in the lands tectonically formed by the Arab and Anatolian plates (Fig. 1). Antakya and a part of the Asi River lie towards the Northeast-Southwest end of the Antakya-Samandağı sediments [31]. This sediment is covered with marine sediments of the Miocene period, Pliocene and Holocene period sediments and also surrounded by normal slip faults from the northeast-southwest margins [32]. Geologically, Antakya is located within the Karasu rift, which has a pre-Pliocene basement and developed in two rock series. The rock series forming the Karasu rift are Paleozoic terrestrial units and Mesozoic allochthonous ophiolitic rock complex [33, 34]. Plio-Quaternary sediments and Quaternary volcanics were emplaced on the Miocene basement. The main fault runs along the Amanos Mountains from Türkoğlu to Antakya [35, 36]. The NNE trending segment is approximately 145 km long and is known as the Amanos fault [37, 38] or the Karasu fault [39]. This fault defines the western border of the Karasu valley and the 30 km wide edge of the Amik plain. This section is filled with Plio-quaternary sediments and is more than 1000 m thick [40]. K-Ar, Nd, Sr and Pb isotopic dating studies have revealed Quaternary age determinations for basaltic rocks along the Karasu valley [34]. Detailed knowledge of near-surface geological conditions is primary importance for understanding empirically measured ground amplifications. The sediments of the Antakya region are basically alluvial units composed of clay, sand and gravel.

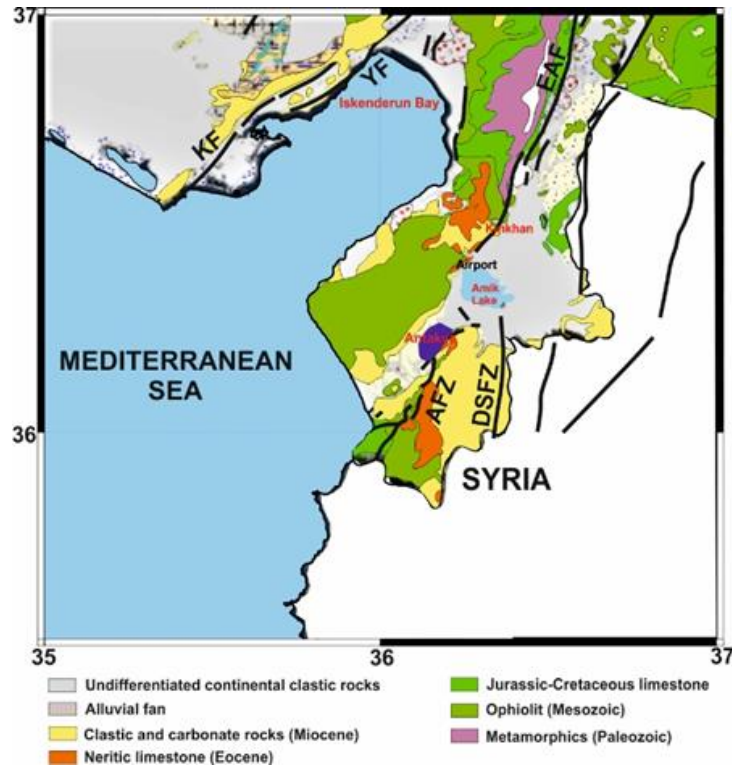


Figure 1. Regional geology map of the study area. The darkblue area shows the Antakya central settlement [41]. EAF: East Anatolian Fault, AFZ: Amanos Fault Zone, DSFZ: Dead Sea Fault Zone, KF: Karasu Fault, YF: Yumurtalık Fault

3. Seismicity and Seismotectonic

Topographically, the urban settlement of Antakya varies. The old settlement was mostly built on the slopes of the Amanos Mountains, which are located to the west and reach 2200 m in height. However, today the development of the city is flatter and has shifted on the alluvium of the Asi River (Fig. 2). The tectonic activity of the region displays a complex tectonic behavior under the influence of faults extending to the Dead Sea, Eastern Anatolia and Cyprus. The study area is the northeast direction Dead Sea Fault Zone (DSFZ), Cyprus-Antakya Transformation Fault, which is the extension of the Cyprus arc coming from the southwest and reaching the Amik Plain through Antakya, and the NNE-SSW trending junction area. The Amanos (or Karasu) Fault is the southern extension of the EAFZ between Türkoğlu (Kahramanmaraş) and Antakya and is an area where tectonic activity takes place continuously. The above-mentioned faults constitute the African/Arabia, Anatolia/Africa and Arabia/Anatolian plate boundaries respectively, forming a triple joint point in the Amik Plain (Fig. 2) [36]. Antakya and its vicinity have been affected by earthquakes for about 2000 years [42- 47]. However, when the earthquake data in this process are examined, considering the frequency of occurrence, the earthquake history of Antakya shows a random distribution that does not show a periodic structure to a large extent [31]. Antakya has also been affected by major earthquakes in historical periods. Some of the severe earthquakes that occurred in the historical period are the earthquakes with intensity $I_0 = X$ and instrumental magnitude $M = 7.5$ that occurred in 245 BC, and $M = 7.5$ and $M = 7.2$ magnitude earthquakes that occurred on 13 August 1822 and 3 April

1872, respectively [44] (Fig. 2). It has been reported that a total of 20,000 people lost their lives in and around Antakya during these earthquakes [48]. When the earthquakes that occurred in the instrumental period are examined, the most important earthquakes were the main shock of $M_b = 5.5$ on 22 January 1997 and the aftershocks of $M = 5.2$ and 5.3 magnitudes. The greatest intensity in these earthquakes was around $I_o = VI-VII$. These earthquakes caused some buildings to collapse or damage. When the focal depths of earthquakes occurring in Antakya and its surroundings are examined, earthquakes occurring along a corridor extending in NNE-SSW direction are generally shallow earthquakes (Fig. 2).

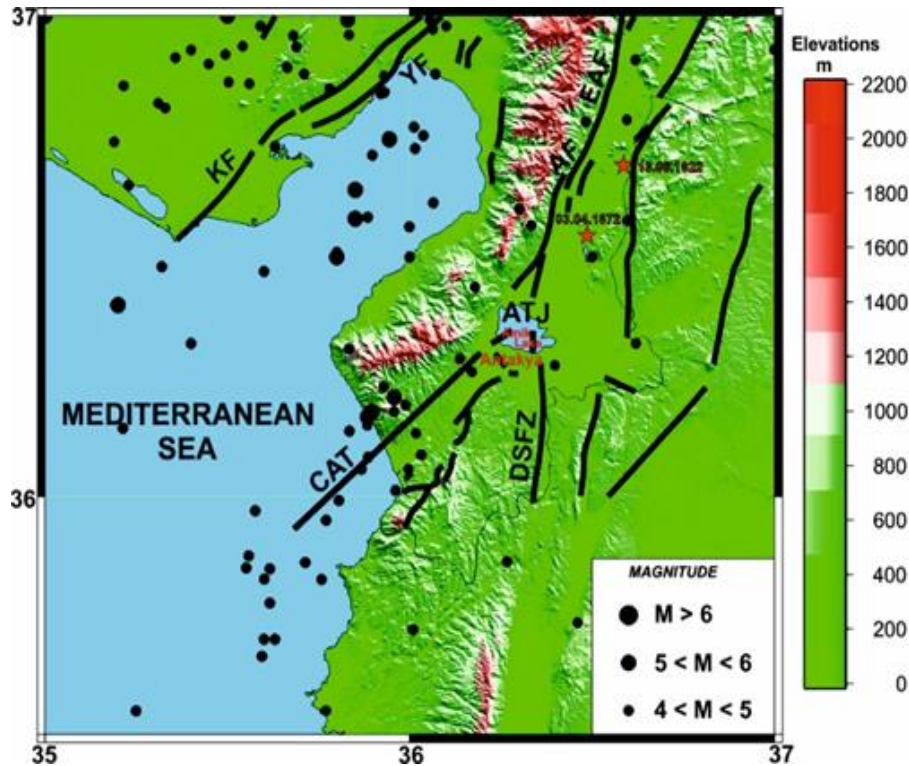


Figure 2. Seismotectonic map of the study area. Red stars show historical earthquakes $M > 7.0$ (Modified from [36]). EAF: East Anatolian Fault, AF: Amanos Fault, DSFZ: Dead Sea Fault Zone, KF: Karasu Fault, YF: Yumurtalık Fault, CAT: Cyprus-Antakya Transform Fault, ATJ: Antakya Triple Junction

The characterization of ground seismic behavior of Antakya city center and its immediate surroundings has been tried to be defined with single station microtremor and refraction microtremor (ReMi) measurements [20]. The spectral analysis of microtremors is a very convenient tool to characterise earthquake site response since it is relatively fast and economic. Large regions can be surveyed in a relatively short period of time. The predominant frequency of horizontal spectra of microtremors is related to local geological conditions. During these studies, the microzonation methodology was applied. The city was divided into cells of $500 \times 500 \text{ m}^2$ and 69 microtremor measurements were taken at the point corresponding to the midpoint of each cell. Predominant frequency and ground amplification variation are investigated [20]. Accordingly, the predominant frequency values vary between 1.25 – 7.96 Hz (average value is 3.21 Hz). Low frequency values are observed especially in the east-northeast

part outside the center of Antakya. While the amplification values fall below 1.0 in some areas in the city center, 3-3.5 times amplification values are seen outside the city center (Fig. 3a).

The ReMi method is applied by using standard P-wave recording equipment and ambient noise to produce average one-dimensional shear-wave profiles. The source of ReMi measurement is composed of traffic and other vehicles, the wind responses of trees, buildings, etc. [49]. The ReMi interpretation and analysis was done using Seisimager/SW software. In the frame of ReMi analysis, there are three steps. The first step is velocity spectral analysis. The basis of the velocity spectral analysis is the p–f transformation. This transformation takes a record section of multiple seismograms, with seismogram amplitudes relative to distance and time (x–t) and converts it to amplitudes relative to the ray parameter p (the inverse of apparent velocity). The second step is Rayleigh Silent segments selection omitting the segments that are influenced by very near noise sources, The ReMi measurements were carried out independently of the microtremor measurements. However, observation points of ReMi measurements were selected around microtremor points to correlate with each other. The third step is shear-wave velocity modelling. The refraction microtremor method interactively forward-models the normal-mode dispersion data picked from the p–f images. The modelling iterates on phase velocity at each frequency, reports when a solution has not been found within the iteration parameters and can model velocity reversals with depth. Shallow and deep ground material information was obtained with the help of boreholes previously drilled [20]. Mainly clayey and sandy units are in the city center and its surroundings, where the effect of the alluvium of the Asi River is observed. It is known that these units turn into claystones in some areas, but continue to the depths, alternating with gravel in most places. Representative geotechnical profiles of the city were prepared and different areas of earthquake sensitivity were compared with each other. V_s velocity values up to 25 m depth were calculated from the records obtained from four strong ground motion recorders in the center of Antakya. In addition, it is understood that the ground period values obtained from microtremor and acceleration measurements are compatible with each other [50]. Considering the V_s values obtained from ReMi measurements, the average V_s velocity values for the first 30 m were calculated (Fig. 3b). These values are particularly structuring pre-shallow foundation design is very important in terms of defining the ground conditions the first 30 meters are important for, in 2019 enacted Turkey Earthquake is also used to define soil classes that are used in conjunction with Hazard Map. The obtained V_{s30} values vary in the range of 324 ms^{-1} to 526 ms^{-1} throughout the study area and show mainly C class and a few points D class ground characteristics. These classifications overlap with the existing drilling information in the study area and are generally represented by medium-tight-very compact sand and solid-hard clay layers.

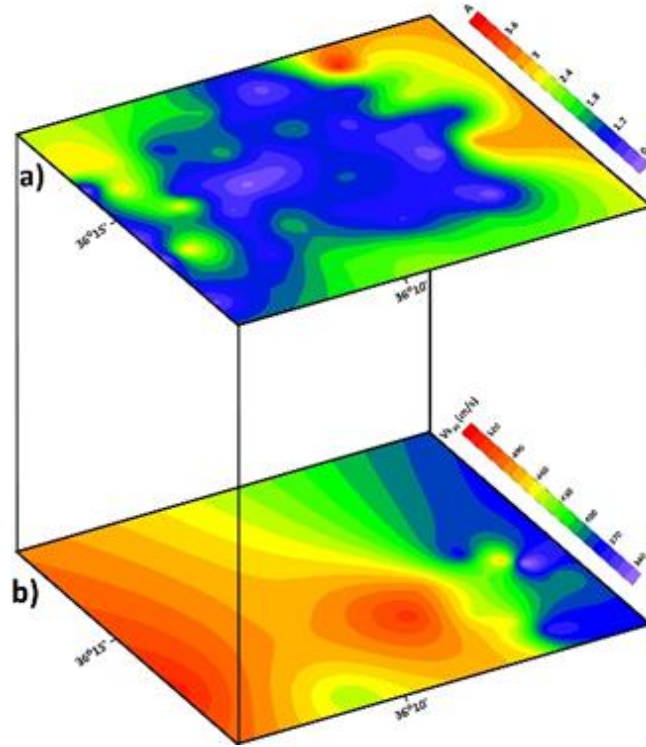


Figure 3. (a) Amplification and (b) V_{s30} map of Antakya [50].

4. Materials and Methods

4.1. Seismic vulnerability index (K_g)

Seismic vulnerability (K_g) is an index that indicates the seismic vulnerability value of a deformed soil layer. Therefore, the Seismic Vulnerability Index is useful for detecting weak zones in unconsolidated sedimentary layers during an earthquake. In this way, it can be demonstrated that there is a good correlation between the seismic fragility of the ground and the distribution of damage caused by the earthquake [51]. Seismic vulnerability index (K_g), which is an important parameter in terms of ground amplification and dominant frequency and structure-ground interaction obtained from microtremor data, changes depending on the soil dynamic properties. In addition, a point-by-point evaluation of the strength or weakness of an area against strong ground motion can also be made with this parameter. The Seismic Vulnerability Index (K_g) can be determined using the amplification (A_o) and predominant frequency (f_o) values at each microtremor measurement point. The formula [52] for calculating K_g can be written as:

$$K_g = \frac{A^2}{f_o} \quad (1)$$

Some destructive earthquakes have K_g values between 20-100 in areas exposed to major damage, and K_g values have 5 or less in areas with less damage [52]. Thus, this parameter (K_g), which is related to the predominant frequency and the amplification coefficient, is used in the estimation of the damage distribution, which can be calculated for both the location and the structure. High unit shear deformation will directly affect the damage. Since the shear wave

velocity of the bedrock is constant, the acceleration in the bedrock and the predominant frequency of the ground above it will determine the damage, in other words, the unit shear deformation that will occur [8, 52]. When we look at the K_g values calculated based on the microtremor measurements made in the city center of Antakya and its surroundings, the presence of vulnerability index exceeding 6 in the northeastern part of the city reveals the vulnerability in this area. The K_g index is higher at low frequency values as expected. It is understood that there is high vulnerability when the K_g index obtained as a result of the calculations made within the scope of this study are lower than 1.3 Hz (Fig. 4).

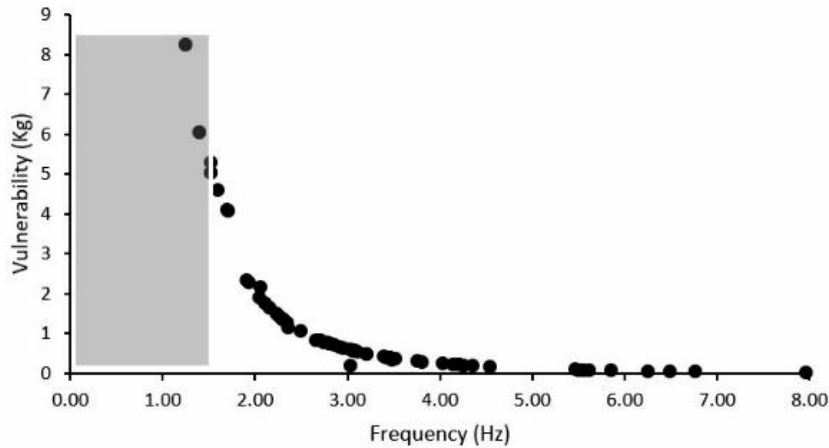


Figure 4. Relationship between vulnerability index and resonant frequency in Antakya. The shaded area shows the vulnerable frequency levels.

Since the average dominant frequency value is 3.21 Hz, the vulnerability expectation of Antakya soils is seen in the east-northeast part and the west border of the area. Especially in the old settlement area, it remains at a very low level. The most important factor for this is the consolidation of the ground over time depending on the density of the settlement Antakya is a very old settlement.

4.2. Calculation of bedrock depth in Antakya

Seismic waves spend a significant part of their travel from the source to the earth surface in the hard bedrock that forms the earth's crust. In the last stage of their travels, they take place within the surface layers called loosely attached soil, which are quite different from the bedrock, and the physical properties of these soil layers largely determine the characteristics of the vibration observed on the earth [53]. Therefore, determination of bedrock depth is one of the critical area investigation stages for seismic hazard analysis. One of the most used common approaches to find bedrock depth is based on the nonlinear regression relationships of bedrock depth with the fundamental resonance frequency [27]. However, these obtained regression relationships are specific to the region. This phenomenon is mainly due to the variation of the average shear velocity according to depth due to different components and different relationships in contrast to the degree of compression of sediments in different regions [54]. It was first demonstrated by [55] and [56] that the thickness of the upper soft sediment layers from another point of view can be determined directly from the predominant frequency obtained by the HVSR of

microtremors. However, the transformation of this relationship into a characteristic formula is described by [57, 58, 59, 60]. Accordingly, the following Eq. (2) was used to obtain bedrock depth (h) using the fundamental resonance frequency (f_{HVSr}).

$$h = a f_{HVSr}^{-b} \quad (2)$$

where a and b are curve fit parameters. V_s values obtained from ReMi measurements made at 15 points and corresponding depth values were obtained. From here, a relationship was established between the predominant frequency value and depth at the points corresponding to the microtremor measurement points. This resulting relationship has been used for other calculated predominant frequencies from microtremor measurement points. A formula that allows the calculation of bedrock depth based on the predominant frequency values obtained from single point station measurements made in the central settlement of Antakya and its vicinity was obtained. An exponential relationship between cover thickness to the bedrock and resonance frequency of site is found and a and b values in Eq. (3) were calculated as

$$H = 101 f_r^{-0.988} \quad (3)$$

Where H is depth of bedrock, f_r is resonant frequency. Statistically the R^2 value is 93.24%, indicating a strong relationship between the frequency and thickness. The depth to be considered as an engineering bedrock has been handled by different sources. [61] considered shear wave velocities of $700 \pm 60 \text{ ms}^{-1}$ with non-penetrating values for 100 impacts in the Standard Penetration Test (SPT) experiment, as the signature of the bedrock representing a stiffer soil column adopted in the design codes of different field classification approaches. According to the shear wave velocity values, the soil of Antakya can be ranged in category C of National Earthquake Hazard Reduction Programme (NEHRP) site classification. Site class C is defined as very dense soil and soft fill, where shear wave velocities are $360 \text{ ms}^{-1} - 760 \text{ ms}^{-1}$ [62]. Nath (2007) [63] defined the engineering bedrock as having a shear wave velocity between 400 ms^{-1} and 700 ms^{-1} for seismic microzonation. Miller et al. (1999) [64] mapped the bedrock using the Multichannel Analysis of Surface Waves (MASW) research, using the shear wave velocity of 244 ms^{-1} as a value for the bedrock. Delgado et al. (2000b) [59], shear wave velocity for Triassic carbonate rocks 250 ms^{-1} and for Triassic - Cretaceous limestones is accepted as geotechnical bedrock. In the surface layer called the ground, the S wave velocity is considered to be less than 760 ms^{-1} and the places where the S wave velocity is greater than 760 ms^{-1} are called engineering bedrock [62]. It is accepted that the dynamic structure of the ground does not change, that is, the S wave velocity values in the region called the engineering bedrock [62, 65]. Nakamura (2008) [8] calculated the depth of foundation along the railway line in Japan and found it as 600 ms^{-1} . Kuo vd. (2016) [66] suggested a value of 600 ms^{-1} as the V_s velocity of the engineering bedrock. In this case, in the formula $f_o = V_s / 4h$ proposed by [8], if the value of f_o and the value of h are substituted, the V_s value can be calculated. The average velocity value reached during this study is around 409 ms^{-1} and ranges between $405-412 \text{ ms}^{-1}$. However, these values are not high enough to be an engineering bedrock. In this case, h values can be obtained by keeping the V_s value constant at 760 ms^{-1} and 600 ms^{-1} velocity values. V_s velocity values can be also calculated for vulnerability situation in Antakya city (Fig. 5). If the soils have V_s velocity below 406 ms^{-1} , they can be vulnerable according to other soils with higher

velocity values. In this case, since the average of the V_{s30} values is 435 ms^{-1} , it is once again understood that the vulnerability effect is quite limited when the first 30 m depth is considered in the study area.

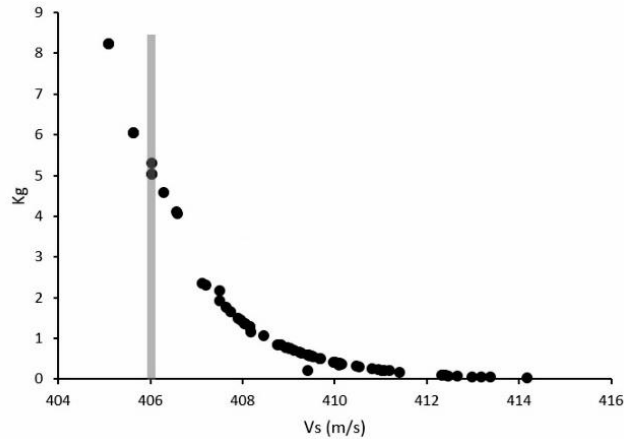


Figure 5. Vulnerability index (K_g) changes versus V_s velocity values in Antakya. The shaded line shows the vulnerability V_s value level.

5. Results and Discussions

Ten seismic design codes came into force in time such as 1940, 1944, 1949, 1953, 1962, 1968, 1975, 1998, 2007, and 2018. The latest seismic code was updated in 2018 and has been put into force since January 2019. Four different earthquake ground motion levels (DD-1, DD-2, DD-3, DD-4) identified in the Turkish Building Earthquake Code [67].

Turkish Earthquake Hazard Map Interactive Web Application (TEHMIWA) has become available for the computation of earthquake parameters used in structural analyses for any geographic location since the beginning of 2019 [68-73]. The comparison of the peak ground acceleration (PGA) and peak ground velocity (PGV) values in fifteen ReMi measurement locations considered within the scope of the study for all earthquake ground motion levels are shown in Table 1 through the TEHMIWA.

Table 1. Comparison of PGA and PGV for different probabilities of exceedance

District	Peak Ground Acceleration (g)-PGA				Peak Ground Velocity (cm/s)-PGV			
	Probability of Exceedance in 50 Years				Probability of Exceedance in 50 Years			
	2%	10%	50%	68%	2%	10%	50%	68%
1	0.843	0.434	0.146	0.099	53.637	26.765	8.251	5.559
2	0.849	0.435	0.146	0.099	53.707	26.765	8.224	5.542
3	0.849	0.436	0.147	0.099	54.082	26.948	8.272	5.567
4	0.849	0.436	0.146	0.098	53.983	26.811	8.215	5.535
5	0.853	0.438	0.146	0.099	54.329	29.980	8.245	5.550
6	0.852	0.438	0.147	0.099	54.303	27.034	8.280	5.570
7	0.851	0.438	0.147	0.100	54.340	27.131	8.339	5.604
8	0.860	0.440	0.147	0.099	54.847	27.186	8.264	5.558
9	0.868	0.444	0.147	0.099	55.417	27.424	8.294	5.571

10	0.859	0.440	0.147	0.099	54.783	27.219	8.297	5.577
11	0.873	0.445	0.147	0.099	55.761	27.525	8.285	5.564
12	0.894	0.453	0.147	0.099	57.155	27.997	8.274	5.545
13	0.895	0.454	0.148	0.099	57.460	28.151	8.326	5.577
14	0.863	0.443	0.148	0.100	55.344	27.485	8.365	5.614
15	0.933	0.468	0.148	0.099	60.055	29.066	8.332	5.560

PGA values were obtained in the range of 0.84-0.93g for the ground motion levels with a probability of exceedance 2% in 50 years for the studied locations, and 0.43-0.47g for a 10% probability of exceedance. The highest PGA was obtained for the location 15, while the lowest PGA was obtained for location 1. Although the locations are closer to each other, there are differences between the values obtained because each location has its own seismic elements. Comparison of the short-period map spectral acceleration coefficient (S_s), the map spectral acceleration coefficient (S_1) for a period of 1.0 seconds, by using different probabilities of exceedance, is shown in Table 2.

Table 2. Comparison of S_s and S_1 obtained for different probabilities of exceedance

District	S_s				S_1			
	Probability of Exceedance in 50 Years				Probability of Exceedance in 50 Years			
	2%	10%	50%	68%	2%	10%	50%	68%
1	2.060	1.023	0.329	0.223	0.557	0.266	0.084	0.057
2	2.066	1.024	0.329	0.222	0.558	0.266	0.084	0.057
3	2.074	1.028	0.330	0.223	0.562	0.268	0.084	0.057
4	2.072	1.026	0.328	0.222	0.560	0.266	0.083	0.056
5	2.083	1.031	0.329	0.223	0.564	0.268	0.084	0.057
6	2.081	1.031	0.330	0.223	0.564	0.269	0.084	0.057
7	2.078	1.033	0.332	0.224	0.566	0.270	0.084	0.057
8	2.100	1.058	0.330	0.223	0.569	0.270	0.084	0.057
9	2.117	1.045	0.331	0.223	0.576	0.272	0.084	0.057
10	2.096	1.037	0.331	0.224	0.569	0.270	0.084	0.057
11	2.129	1.049	0.331	0.223	0.579	0.273	0.084	0.057
12	2.178	1.067	0.331	0.223	0.592	0.276	0.084	0.057
13	2.181	1.069	0.332	0.224	0.597	0.278	0.084	0.057
14	2.107	1.045	0.333	0.225	0.577	0.273	0.085	0.057
15	2.269	1.101	0.333	0.224	0.622	0.286	0.085	0.057

Also, within the scope of the study, earthquake parameters were calculated for different probabilities of exceedance. In this context, local ground coefficients (F_s and F_1), short period design spectral acceleration coefficient (S_{Ds}) for 0.2 s and design spectral acceleration coefficient (S_{D1}) for 1.0 s, horizontal design spectrum corner periods (T_A and T_B) and vertical design spectrum corner periods (T_{AD} and T_{BD}) were obtained separately for each location. The earthquake parameter obtained for the earthquake ground motion level with a probability of

exceedance 2% in 50 years for fifteen different points determined by local soil class land measurements are shown in Table 3.

Table 3. Earthquake parameter values according to the probability of exceedance 2%.

No	F _s	F ₁	S _{Ds}	S _{D1}	T _A	T _B	T _{AD}	T _{BD}
1	1.200	1.443	2.472	0.804	0.065	0.325	0.022	0.108
2	1.000	1.742	2.066	0.972	0.094	0.470	0.031	0.157
3	1.000	1.738	2.074	0.977	0.094	0.471	0.031	0.157
4	1.200	1.440	2.486	0.806	0.065	0.324	0.022	0.108
5	1.200	1.436	2.500	0.810	0.065	0.324	0.022	0.108
6	1.200	1.436	2.497	0.810	0.065	0.324	0.022	0.108
7	1.200	1.434	2.494	0.812	0.065	0.325	0.022	0.108
8	1.200	1.431	2.520	0.814	0.065	0.323	0.022	0.108
9	1.200	1.424	2.540	0.820	0.065	0.323	0.022	0.108
10	1.000	1.731	2.096	0.985	0.094	0.470	0.031	0.157
11	1.200	1.421	2.555	0.823	0.064	0.322	0.021	0.107
12	1.200	1.408	2.614	0.834	0.064	0.319	0.021	0.106
13	1.200	1.403	2.617	0.838	0.064	0.320	0.021	0.107
14	1.200	1.423	2.528	0.821	0.065	0.325	0.022	0.108
15	1.200	1.400	2.723	0.871	0.064	0.320	0.021	0.107

The earthquake parameter obtained for the earthquake ground motion level with a probability of exceedance 10% in 50 years are shown in Table 4.

Table 4. Earthquake parameter values according to the probability of exceedance 10%.

No	F _s	F ₁	S _{Ds}	S _{D1}	T _A	T _B	T _{AD}	T _{BD}
1	1.200	1.500	1.228	0.399	0.065	0.325	0.022	0.108
2	1.090	2.068	1.117	0.550	0.099	0.493	0.033	0.164
3	1.089	2.064	1.119	0.553	0.099	0.494	0.033	0.165
4	1.200	1.500	1.271	0.399	0.065	0.324	0.022	0.108
5	1.200	1.500	1.237	0.402	0.065	0.325	0.022	0.108
6	1.200	1.500	1.237	0.403	0.065	0.326	0.022	0.109
7	1.200	1.500	1.240	0.405	0.065	0.327	0.022	0.109
8	1.200	1.500	1.246	0.405	0.065	0.325	0.022	0.108
9	1.200	1.500	1.254	0.408	0.065	0.325	0.022	0.108
10	1.085	2.060	1.125	0.556	0.099	0.494	0.033	0.165
11	1.200	1.500	1.259	0.410	0.065	0.325	0.022	0.108
12	1.200	1.500	1.280	0.424	0.065	0.323	0.022	0.108
13	1.200	1.500	1.283	0.417	0.065	0.325	0.022	0.108
14	1.200	1.500	1.254	0.410	0.065	0.327	0.022	0.109
15	1.200	1.500	1.321	0.429	0.065	0.325	0.022	0.108

The earthquake parameter values obtained for the earthquake ground motion level with a probability of exceedance 50% in 50 years are shown in Table 5.

Table 5. Earthquake parameter values according to the probability of exceedance 50%.

No	F _s	F ₁	S _{Ds}	S _{D1}	T _A	T _B	T _{AD}	T _{BD}
----	----------------	----------------	-----------------	-----------------	----------------	----------------	-----------------	-----------------

1	1.300	1.500	0.428	0.126	0.059	0.295	0.020	0.098
2	1.537	2.400	0.506	0.202	0.080	0.399	0.027	0.133
3	1.536	2.400	0.507	0.202	0.080	0.398	0.027	0.133
4	1.300	1.500	0.426	0.124	0.058	0.292	0.019	0.097
5	1.300	1.500	0.428	0.126	0.059	0.295	0.020	0.098
6	1.300	1.500	0.429	0.126	0.059	0.294	0.020	0.098
7	1.300	1.500	0.432	0.126	0.058	0.292	0.019	0.097
8	1.300	1.500	0.429	0.126	0.059	0.294	0.020	0.098
9	1.300	1.500	0.430	0.126	0.059	0.293	0.020	0.098
10	1.535	2.400	0.508	0.202	0.079	0.397	0.026	0.132
11	1.300	1.500	0.430	0.126	0.059	0.293	0.020	0.098
12	1.300	1.500	0.430	0.126	0.059	0.293	0.020	0.098
13	1.300	1.500	0.432	0.126	0.058	0.292	0.019	0.097
14	1.300	1.500	0.433	0.127	0.059	0.295	0.020	0.098
15	1.300	1.500	0.433	0.127	0.059	0.295	0.020	0.098

The earthquake parameter values obtained for the earthquake ground motion level with a probability of exceedance 50% in 50 years are shown in Table 6.

Table 6. Earthquake parameter values according to probability of exceedance 68%

No	F _s	F ₁	S _{Ds}	S _{D1}	T _A	T _B	T _{AD}	T _{BD}
1	1.300	1.500	0.290	0.086	0.059	0.295	0.020	0.098
2	1.600	2.400	0.355	0.137	0.077	0.385	0.026	0.128
3	1.600	2.400	0.357	0.137	0.077	0.383	0.026	0.128
4	1.300	1.500	0.289	0.084	0.058	0.291	0.019	0.097
5	1.300	1.500	0.290	0.086	0.059	0.295	0.020	0.098
6	1.300	1.500	0.290	0.086	0.059	0.295	0.020	0.098
7	1.300	1.500	0.291	0.086	0.059	0.294	0.020	0.098
8	1.300	1.500	0.290	0.086	0.059	0.295	0.020	0.098
9	1.300	1.500	0.290	0.086	0.059	0.295	0.020	0.098
10	1.600	2.400	0.358	0.137	0.076	0.382	0.025	0.127
11	1.300	1.500	0.290	0.086	0.059	0.295	0.020	0.098
12	1.300	1.500	0.290	0.086	0.059	0.295	0.020	0.098
13	1.300	1.500	0.291	0.086	0.059	0.294	0.020	0.098
14	1.300	1.500	0.292	0.086	0.058	0.292	0.019	0.097
15	1.300	1.500	0.291	0.086	0.059	0.294	0.020	0.098

The comparison of the elastic design spectra obtained for the earthquake ground motion level with a probability of exceeding 10% in 50 years for fifteen different locations considered within the scope of the study is shown in Fig. 6.

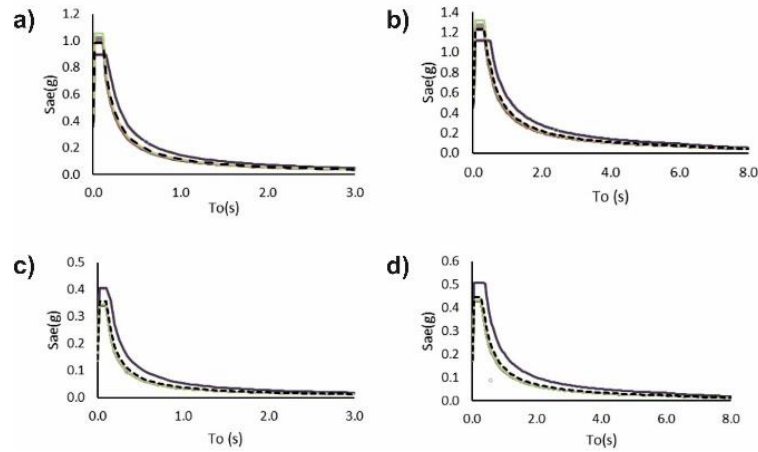


Figure 6. Comparison of spectra obtained for DD-2 and DD-3 ground motion level. (a) DD-2 Vertical (b) DD-2 Horizontal (c) DD-3 Vertical (d) DD-3 Horizontal

There are differences between the design spectra obtained according to different geographic locations with the same local ground conditions. In addition, these differences appear more clearly when local ground conditions change. The change in design spectra will affect the target displacement values expected from the structures. In this context, analysis and evaluation of the structures are more realistic by using site-specific design spectra [74]. The maximum shear strain is obtained by proportioning PGV and mean V_s value [75] Eq. 4. In this study, the value of V_{s30} was taken as the average value of V_s .

$$\gamma_{\max} = \text{PGV} / V_{s\text{-Average}} \quad (4)$$

While the PGA value represents shear stress, the PGV value represents the maximum shear strain. When the V_{s30} distribution of the ground properties of Antakya central settlement is examined and when we calculate the γ_{\max} value from the Eq. 4, the results in Table 8 are obtained. In addition, the average strain (I_γ) calculation has been made according to [76] (Eq. 5).

$$I_\gamma = \left(\frac{M-1}{10} \right) \times \left(\frac{\text{PGV}}{V_{s30}} \right) \times 100\% \quad (5)$$

Here I_γ is the average strain, M : Moment magnitude, V_{s30} : the average distribution of 30 m of V_s . With the help of this relation, the I_γ distribution was calculated with an alternation of 0.5 for earthquakes in the range of 5.0-7.5 (Table 7). According to the Turkish Building Earthquake Code [67], considering the Earthquake Ground Motion levels, the earthquake ground motion level DD-3, where the probability of exceedance, the spectral magnitudes in 50 years is 50% and the corresponding recurrence period is 72 years statistically, is for Antakya earthquakes. Therefore, the screenings were made according to DD-3.

Table 7. Calculation of I_γ % depending on the γ_{\max} change of earthquakes between 5.0 - 7.5 Magnitudes.

γ_{\max}	I_γ %					
	M=5.0	M=5.5	M=6.0	M=6.5	M=7.0	M=7.5

0.020525	0.820995	0.923619	1.026244	1.128868	1.231493	1.334117
0.022972	0.918883	1.033743	1.148603	1.263464	1.378324	1.493184
0.025531	1.021235	1.148889	1.276543	1.404198	1.531852	1.659506
0.017743	0.709719	0.798434	0.887149	0.975864	1.064579	1.153294
0.018121	0.724835	0.81544	0.906044	0.996648	1.087253	1.177857
0.017322	0.692887	0.779498	0.866109	0.95272	1.039331	1.125941
0.022003	0.880106	0.990119	1.100132	1.210145	1.320158	1.430172
0.018529	0.741166	0.833812	0.926457	1.019103	1.111749	1.204395
0.017101	0.684041	0.769546	0.855052	0.940557	1.026062	1.111567
0.022424	0.896973	1.009095	1.121216	1.233338	1.345459	1.457581
0.016056	0.642248	0.722529	0.80281	0.883091	0.963372	1.043653
0.018805	0.752182	0.846205	0.940227	1.03425	1.128273	1.222295
0.017603	0.704101	0.792114	0.880127	0.96814	1.056152	1.144165
0.020012	0.800478	0.900538	1.000598	1.100658	1.200718	1.300778
0.01584	0.633612	0.712814	0.792015	0.871217	0.950418	1.02962

As the magnitude of the earthquake increases, lateral displacement will naturally increase. However, in areas where the V_{s30} value is low, approximately 0.6% displacement increase is quite significant. When the I_γ distribution map, which was created considering the largest expected earthquake ($M = 7.0$) in the study area, is examined, a greater strain effect is observed in the east of the area compared to other areas (Fig. 7). This result overlaps with other information.

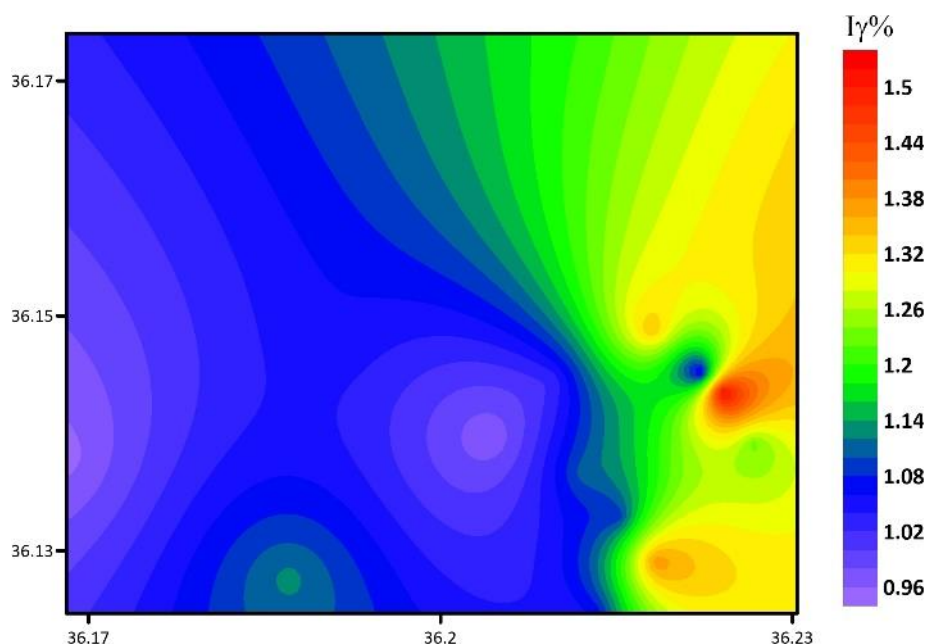


Figure 7. Distribution of I_γ % in Antakya

Determination of the bedrock depth is one of the critical field investigation stages of the underground behaviors that can be encountered especially during an earthquake, depending on the seismic hazard analysis and the differentiation of the bedrock depths. In this study, an experimental relationship was obtained between the resonance frequencies of the H/V spectra

based on single station microtremor measurements and the depth of the bedrock in Antakya. First of all, the fundamental variable in establishing this relationship is the resonance frequency. It is possible to have an idea about the ground according to the greatness of fundamental resonance frequency ($f_{HVS\text{R}}$), as it reflects the ground behavior properties [77]. However, the values of the frequency depend not only on the character of the ground, but also on the depth of the ground. In conditions where the soil is thick, in other words, the depth of the bedrock is deep, this situation should also be considered during the evaluation. Thus, in an area with a low resonance frequency, it is not only possible to talk about the loose soil structure, but also to consider the bedrock depth information. In this sense, the coefficients should come into play as a factor of the depth while using the relation where the bedrock depth is obtained from the resonant frequency. The depth of bedrock for Antakya varies between 21-73 m. This information is in agreement with the values around the Amik Plain in the [78] publication obtained from the regional study. While a relatively shallow bedrock depth is obtained in the center of Antakya, it is seen that the depths outside Antakya increase.

The findings obtained in this analysis are compatible with the Antakya microzonation map prepared by [20]. In the center of Antakya, this map shows that the predominant period is tiny, while the dominant period rises towards the peripheral areas of the city. The authors attributed this high value of the predominant period to the looser soil in the peripheral than the soil in the center of Antakya. This current study showed that the high value of the ground vibration period was due not only to the loose ground, but also to the loose ground thickness. In other words, it is seen that the bedrock around Antakya is deeper than the center and therefore the dominant frequency is lower at the peripheral than the center (Fig. 8).

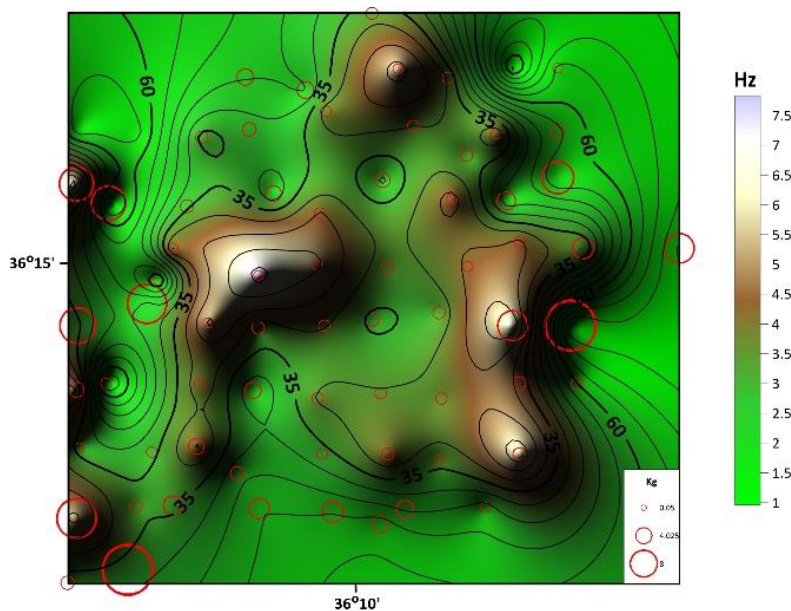


Figure 8. Presentation of predominant frequency, bedrock depth and vulnerability index.

The vulnerability limit for Antakya soils should be considered as soils with V_s velocity lower than 406 ms^{-1} . This situation reveals a threshold value definition, especially in defining lateral resistance (Fig. 8). The map in Figure 8, where the obtained results are shown together, shows

that the depth of the bedrock is reduced in high frequency areas and the vulnerability index is low. On the other hand, it is observed that the depth of bedrock increases and vulnerability index increases in soils away from the center where the dominant frequency drops.

Contour values show the depth of bedrock. The prevailing frequency distribution varies from white to green. White-brown colors indicate high frequencies; green colors indicate low frequencies. Red circles indicate vulnerability.

6. Conclusions

The depth of bedrock for Antakya varies between 21-73 m. While a relatively shallow bedrock depth is obtained in the center of Antakya, it is seen that the depths outside Antakya increase. This study showed that the high value of the ground vibration period was due not only to the loose ground, but also to the loose ground thickness. In other words, it is seen that the bedrock around Antakya is deeper than the center and therefore the dominant frequency is lower at the peripheral than the center. The vulnerability limit for Antakya soils should be considered as soils with V_s velocity lower than 406 ms^{-1} . This situation reveals a threshold value definition, especially in defining lateral resistance. It means, the depth of the bedrock is reduced in high frequency areas and the vulnerability index is low. On the other hand, it is observed that the depth of bedrock increases and vulnerability index increases in soils away from the center (northeastern part of the area) where the dominant frequency drops. Soil class was obtained as C for Antakya and D for loose areas.

Ethics in Publishing

There are no ethical issues regarding the publication of this study.

Author Contributions

Aydın Büyüksaraç made statistical and seismic analyzes of the study. Özcan Bektaş made statistical and seismic analyzes of the study. Ercan Işık collected data, planned, and designed the analysis. Semir Över made seismotectonical investigation. Selçuk Kaçın made vulnerability analyzes.

References

- [1] Hadzima-Nyarko, M. and Kalman Sipos, T. 2017. "Insights from existing earthquake loss assessment research in Croatia", *Earthq. Struct.*, 13(4), 365-375.
- [2] Işık, E., Işık, M.F. and Bülbül, M.A. 2017. "Web based evaluation of earthquake damages for reinforced concrete buildings", *Earthq. Struct.*, 13(4), 387-396.
- [3] Strukar, K., Sipos, T. K., Jelec, M. and Hadzima-Nyarko, M. 2019. "Efficient damage assessment for selected earthquake records based on spectral matching", *Earthq. Struct.*, 17(3), 271-282.

- [4] Balan, S.F., Tiganescu, A., Apostol, B.F., Danet, A. 2020. “Post-earthquake warning for Vrancea seismic source based on code spectral acceleration exceedance”, *Earthq. Struct.*, 17(4), 365-372.
- [5] Pavić, G., Hadzima-Nyarko, M., and Bulajić, B. 2020. “A Contribution to a UHS-based Seismic Risk Assessment in Croatia—A Case Study for the City of Osijek”, *Sustainability-Basel*, 12(5), 1796.
- [6] Xian, L., He, Z. and Ou, X. 2016. “Incorporation of collapse safety margin into direct earthquake loss estimate”, *Earthq. Struct.*, 10(2), 429-450.
- [7] Isik, E. 2016. “Consistency of the rapid assessment method for reinforced concrete buildings”, *Earthq. Struct.*, 11(5), 873-885.
- [8] Nakamura, Y. 2008. “On the H/V spectrum”, *The 14th World Conf. on Earthquake Engineering*, Beijing, China, 12–17 October.
- [9] Nakamura, Y. 1989. “A method for dynamic characteristics estimations of subsurface using microtremors on the ground surface”, *Q Rep RTRI Jpn*, 30, 25–33.
- [10] Field, E. H., and Jacob, K. 1993. “The theoretical response of sedimentary layers to ambient seismic noise”, *Geophys Res Lett*, 20–24, 2925–2928.
- [11] Lachet, C., Bard, P.Y. 1994. “Numerical and theoretical investigations on the possibilities and limitations of Nakamura’s technique”, *J Phys Earth*, 42, 377–397.
- [12] Lermo, J., Chavez-Garcia, F. J. 1994. “Are microtremors useful in site response evaluation?”, *B Seismol Soc Am*, 84, 1350–1364.
- [13] Bindi, D., Parolai, S., Spallarossa, D., and Cattaneo, M. 2000. “Site effects by H/V ratio: Comparison of two different procedures”, *J Earthq Eng*, 4, 97–113.
- [14] Fah, D., Kind, F., Giardini, D. 2001. “A theoretical investigation of average H/V ratios”, *Geophys J Int*, 145, 535–549.
- [15] Bard, P. Y., and SESAME team. 2004. “Guidelines for the implementation of the H/V spectral ratio technique on ambient vibrations: Measurements, processing and interpretation”, *SESAME European research project*, WP12—Deliverable D23. 12.
- [16] Bonnefoy-Claudet, S., Cornou, C., Bard, P.-Y., Cotton, F., Moczo, P., Kristek, J., Fah, D. 2006. “H/V ratio: a tool for site effects evaluation, results from 1-D noise simulations”, *Geophys J Int*, 167, 827–837.
- [17] Molnar, S., Cassidy, J. F., Castellaro, S., Cornou, C., Crow, H., Hunter, J. A., Matsushima, S., Sánchez-Sesma, F. J., and Yong, A. 2018. “Application of Microtremor Horizontal-to-Vertical Spectral Ratio (MHVSR) Analysis for Site Characterization: State of the Art”, *Surv Geophys*, 39, 613–631.

- [18] Pilz, M., Parolai, S., Leyton, F., Campos, J., Zschau, J. 2009. “A comparison of site response techniques using earthquake data and ambient seismic noise analysis in the large urban areas of Santiago de Chile”, *Geophys J Int*, 178(2), 713–728,
- [19] Hunter, J.A., Crow, H.L. 2012. “Shear wave velocity measurement guidelines for Canadian seismic site characterization in soil and rock”, *Geol Surv of Canada*, Open File 7078, p. 227.
- [20] Över, S., Büyüksaraç, A., Bektaş, O. and Filazi, A. 2011. “Assessment of potential seismic hazard and site effect in Antakya (Hatay Province), SE Turkey”, *Environ Earth Sci*, 62, 313-326.
- [21] Büyüksaraç, A., Bektaş, O., Yılmaz, H., Arısoy, M.O. 2013. “Preliminary seismic microzonation of Sivas city Turkey using microtremor and refraction microtremor ReMi measurements”, *J. Seismol.*, 17, 425–435.
- [22] Akkaya, İ. 2015. “The application of HVSR microtremor survey method in Yüksekova (Hakkari) region, Eastern Turkey”. *J African Earth Sci*, 109, 87-95.
- [23] Akın, Ö. and Sayıl, N. 2016. “Site characterization using surface wave methods in the Arsin-Trabzon province, NE Turkey”. *Environ Earth Sci*, 75, 72.
- [24] Rezaei, S. and Choobbasti, A. J. 2018. “Evaluation of local site effect from microtremor measurements in Babol City, Iran”, *J Seismol*, 22, 471–486.
- [25] Bekler, T., Demirci, A., Ekinçi, Y.L., Büyüksaraç, A. 2019. “Analysis of local site conditions through geophysical parameters at a city under earthquake threat: Çanakkale, NW Turkey”, *J Appl Geophys*, 63, 31-39.
- [26] Gupta, R. K., Agrawal, M., Pal, S. K., Kumar, R., and Srivastava, S. 2019. “Site characterization through combined analysis of seismic and electrical resistivity data at a site of Dhanbad, Jharkhand, India”, *Environ Earth Sci*, 78, 226.
- [27] Thabet, M. 2019. “Site-Specific Relationships between Bedrock Depth and HVSR Fundamental Resonance Frequency Using KiK-NET Data from Japan”, *Pure Appl. Geophys*.
- [28] Büyüksaraç, A., Bekler, T., Demirci, A., Eyisüren, O. 2021a. “New insights into the dynamic characteristics of alluvial media under the earthquake prone area: a case study for the Çanakkale city settlement (NW of Turkey)”, *Arabian J Geosci.*, 14, 2086
- [29] Büyüksaraç, A., Karaca, Ö., Eyisüren, O., Bektaş, Ö., Işık, E. 2022. “Importance of Bedrock Depth Knowledge in Basins: Çanakkale (Dardanelles) Case History”, In: *Glavaš, H., Hadzima-Nyarko, M., Karakašić, M., Ademović, N., Avdaković, S. (eds) 30th International Conference on Organization and Technology of Maintenance (OTO 2021). OTO 2021. Lecture Notes in Networks and Systems*, vol 369. Springer, Cham.
- [30] Özdağ, Ö.C., Gönenç, T., and Akgün, M. 2015. “Dynamic amplification factor concept of soil layers: a case study in İzmir (Western Anatolia)”, *Arab J Geosci*, 8, 10093–10104.

- [31] Beyen, K., Erdik, M., Mazmanoğlu, C., Ekmekçiöğlü, Z. 2003. “Antakya’nın geçmişten günümüze sismik aktivitesi ve yapılması gerekenlerin bir uluslararası konferansın ışığında değerlendirilmesi”, *TMH- Türkiye Mühendislik Haberleri*, 423, 51-53.
- [32] Tarı, U., Tüysüz, O., Genç, Ş.C., İmren, C., Blackwell, B.A.B., Lom, N., Tekeşin, Ö., Üsküplü, S., Erel, L., Altıok, S., Beyhan, M. 2013. “The geology and morphology of the Antakya Graben between the Amik Triple Junction and the Cyprus Arc”, *Geodinamica Acta*, 26(1-2), 27-55.
- [33] Tekeli O., Aksay, A., Urgan, B.M., and Işık, A. 1983. “Geology of the Aladağ Mountains. In: Tekeli, O. and Göncüoğlu, M.C. (eds) Geology of the Taurus Belt”, *Proceedings of International Symposium*, Ankara (Turkey), 143-158.
- [34] Rojay, B., Heimann, A. and Toprak, V. 2001. “Neotectonic and volcanic characteristics of the Karasu Fault zone (Anatolia, Turkey): The transition zone between the Dead Sea transform and the East Anatolian fault zone”, *Geodinamica Acta*, 14, 197–212.
- [35] Şaroğlu, F., Emre, Ö., and Kuşçu, İ. 1992. “The East Anatolian fault zone of Turkey”, *Anales Tectonicae*, VI, 99–125.
- [36] Över, S., Kavak, K.Ş., Bellier, O., and Özden, S. 2004. “Is the Amik Basin (SE-Turkey) a Triple Junction Area? Analyses of SPOT XS Imagery and Seismicity”, *Int J Remote Sensing*, 25(19), 3857-3872.
- [37] Lyberis, N., Yurur, T., Chorowicz, J., Kasapoglu, E. and Gundogdu, N. 1992. “The East Anatolian fault: an oblique collisional belt”, *Tectonophysics*, 204, 1–15.
- [38] Över, S., Ünlügenç, UC., and Bellier, O. 2002. “Quaternary stress regime change in the Hatay region (SE-Turkey)”, *Geophys J Int*, 148, 646-662.
- [39] Westaway, R. 1994. “Present-day kinematics of the Middle East and eastern Mediterranean”, *J Geophys Res.*, 99 (B6), 12071-12090.
- [40] Perinçek, D. and Eren, A.G. 1990. “Doğrultu atımlı Doğu Anadolu ve Ölü Deniz fay zonları etki alanında gelişen Amik havzasının kökeni”, *Türkiye 8. Petrol Kongresi Bildiri Kitabı*, 180–192.
- [41] Akbaş, B., Akdeniz, N., Aksay, A., Altun, İ.E., Balcı, V., Bilginer, E., Bilgiç, T., Duru, M., Ercan, T., Gedik, İ., Günay, Y., Güven, İ.H., Hakyemez, H.Y., Konak, N., Papak, İ., Pehlivan, Ş., Sevin, M., Şenel, M., Tarhan, N., Turhan, N., Türkecan, A., Ulu, Ü., Uğuz, M.F., Yurtsever, A. 2011. “1:1.250.000 ölçekli Türkiye Jeoloji Haritası”, *Maden Tetkik ve Arama Genel Müdürlüğü Yayını*, Ankara-Türkiye.
- [42] Willis, B. 1928. “Earthquakes in the Holy Land”, *B Seismol Soc Am*, 18 (2): 73–103.
- [43] Sieberg, A. 1932. “Erdbebengeographie”, *Band IV, Lieferung 3, Verlag von Gebrüder Borntraeger*, Berlin.

- [44] Ergin, K., Guclu, U., Uz, Z. 1967. “A catalogue of earthquakes of Turkey and surrounding area (11 AD to 1964 AD)”, *Maden Fakultesi, Arz Fizigi Enstitusu Yayınları*, Istanbul. 24, 1-28.
- [45] Ambraseys, N.N. 1970. “Some characteristic features of the Anatolian fault zone”, *Tectonophysics*, 9, 143–165.
- [46] Ambraseys, N.N. 1989. “Temporary seismic quiescence: SE Turkey”, *Geophys J Int*, 96, 311–331.
- [47] Soysal, H., Sipahioglu, S., Kolcak, D. and Altinok, Y. 1981. “Turkiye tarihsel deprem kataloğu”, *TUBITAK Project (No: TBAG-341)*, Ankara.
- [48] Kalafat, D. and Bagci, G. 2001. “Adana ve Doğu Anadolu fay zonunun depremsellik özellikleri”. TMMOB, *Jeofizik Mühendisleri toplantısı*, Adana, 36-43.
- [49] Louie, J.N. 2001. “Faster, Better: Shear-wave velocity to 100 meters depth from refraction microtremor arrays”, *Bull Seism Soc Am*, 91, 347–364.
- [50] Büyüksaraç, A., Över, S., Geneş, M.C., Bikçe, M., Kaçın, S., Bektaş, Ö. 2014. “Estimating shear wave velocity using acceleration data in Antakya (Turkey)”, *Eart Sci. Res. J.*, 18(2), 99 – 105.
- [51] Nakamura, Y. 1997. “Vulnerability indexes for surface ground and structures using microtremor”, *8th Soil Dynamics Earthquake Engineering '97*, Istanbul, Turkey, 20–24 July.
- [52] Nakamura, Y. 2000. “Clear identification of fundamental idea of Nakamura’s technique and its application”, in *Proceedings of the XII world conference earthquake engineering*. Auckland, New Zealand, 8.
- [53] Yalçınkaya, E., Serhat Tekebaş, S., and Pınar, A. 2013. “Analysis of ambient noise in Yalova, Turkey: discrimination between artificial and natural excitations”, *J Seismol.*, 17, 1021–1039.
- [54] Liang, D., Gan, F., Zhang, W., and Jia, L. 2018. “The application of HVSR method in detecting sediment thickness in karst collapse area of Pearl River Delta, China”, *Environ Earth Sci*, 77, 259.
- [55] Yamanaka, H., Takemura, M., Ishida, H., Niwa, M. 1994. “Characteristics of long-period microtremors and their applicability in exploration of deep sedimentary layers”, *B Seismol Soc Am*, 84, 1831–1841.
- [56] Field, E. H. 1996. “Spectral amplification in a sediment-filled valley exhibiting clear basin-edge-induced waves”, *B Seismol Soc Am*, 86, 991–1005.
- [57] Ibs-von Seht, M., Wohlenberg, J., 1999. Microtremor measurements used to map thickness of soft sediments. *Bulletin of the Seismological Society of America* 89, 250–259.

- [58] Delgado, J., Casado, C. L., Estevez, A., Giner, J., Cuenca, A., Molina, S. 2000a. “Mapping soft soils in the Segura River valley (SE Spain): A case study of microtremors as an exploration tool”, *J Appl Geophys*, 45, 19–32.
- [59] Delgado, J., Casado, C. L., Giner, J., Estevez, A., Cuenca, A., Molina, S. 2000b. “Microtremors as a geophysical exploration tool: Applications and limitations”, *Pure Appl Geophys*, 157, 1445–1462.
- [60] Parolai, S., Bormann, P., Milkereit, C. 2002. “New relationships between Vs, thickness of sediments, and resonance frequency calculated by the H/V ratio of seismic noise for Cologne Area (Germany)”, *B Seismol Soc Am*, 92, 2521–2527.
- [61] Anbazhagan, P., Sitharam, T. G. (2009), “Spatial variability of the depth of weathered and engineering bedrock using multichannel analysis of surface wave method”. *Pure Appl Geophys*, 166, 409–428.
- [62] FEMA 450. 2004. “NEHRP recommended provisions for seismic regulations for new buildings and other structures”, 2003 edition, part 1—provisions (p. 356), *National Institute of Building Sciences*, Washington, D.C.: Building Seismic Safety Council.
- [63] Nath, S.K. 2007. “Seismic microzonation framework—principles and applications”, in *Proceedings of the workshop on microzonation, Indian Institute of Science, Bangalore*, 26–27 June 2007, India, pp. 9–35.
- [64] Miller, R. D., Xia, J., Park, C. B., Ivanov, J. 1999. “Multichannel analysis of surface waves to map bedrock”, *The Leading Edge*, 18(12), 1392–1396.
- [65] Kramer, S. L. 1996. “Geotechnical Earthquake Engineering”, *Prentice Hall*, 653 pp
- [66] Kuo, C., Chen, C., Lin, C., Wen, K., Huang, J., Chang, S.J. 2016. “S-wave velocity structure and site effect parameters derived from microtremor arrays in the Western Plain of Taiwan”, *J. Asian Earth Sci*, 128(1), 27-41.
- [67] TBDY, 2018. Türkiye Bina Deprem Yönetmeliği, Afet ve Acil Durum Yönetimi Başkanlığı, Ankara
- [68] DEMP 2020. “Interactive earthquake map web page for the 08.06.2020 available at <https://tdth.afad.gov.tr/>”
- [69] Çeken, U., Dalyan, İ., Kılıç, N., Köksal, T.S., Tekin, B.M. 2017. “Türkiye Deprem Tehlike Haritaları İnteraktif Web Uygulaması”, 4. *In Proceedings of the International Earthquake Engineering and Seismology Conference*, Bucharest, Romania.
- [70] Akkar, S., Kale, Ö., Yakut, A., and Ceken, U. 2018. “Ground-motion characterization for the probabilistic seismic hazard assessment in Turkey”, *B. Earthq. Eng.*, 16(8), 3439-3463.

- [71] Işık, E., Büyüksaraç, A., Ekinci, Y. L., Aydın, M. C., and Harirchian, E. 2020. “The effect of site-specific design spectrum on earthquake-building parameters: a case study from the Marmara Region (NW Turkey)”, *Appl. Sci.*, 10(20), 7247.
- [72] Işık, E., Ekinci, Y. L., Sayıl, N., Büyüksaraç, A., and Aydın, M. C. 2021. “Time-dependent model for earthquake occurrence and effects of design spectra on structural performance: a case study from the North Anatolian Fault Zone, Turkey”, *Turkish J Earth Sci*, 30(2), 215-234.
- [73] Büyüksaraç, A., Işık, E., Harirchian, E. 2021b. “A case study for determination of seismic risk priorities in Van (Eastern Turkey)”, *Earthq. Struct.*, 20(4), 445-455.
- [74] Işık, E., Kutanis, M., and Bal, İ. E. 2016. “Displacement of the buildings according to site-specific earthquake spectra”, *Period Polytech-Civ*, 60(1), 37-43.
- [75] Idriss, I.M. 2014. “An NGA-West2 empirical model for estimating the horizontal spectral values generated by shallow crustal earthquakes”, *Earthq. Spectra*, 30, 1155–1177.
- [76] Kwak, D.Y., Seyhan, E. 2020. “Two-stage nonlinear site amplification modeling for Japan with V and fundamental frequency dependency”, *Earthq Spectra*, 1–27,
- [77] Birgören, G., Özel, O., Siyahi, B. 2009. “Bedrock depth mapping of the coast south of Istanbul: Comparison of analytical and experimental analyses”, *Turkish J Earth Sci*, 18, 315–329.
- [78] Pamuk E. and Ozer C. 2020. “The Site Effect Investigation with Using Horizontal-to-Vertical Spectral Ratio Method on Earthquake Data, South of Turkey”, *Geotectonics*, 54(4), 563–576.